

grates from the point of contact to generate this structure, this type of proof-of-concept experiment is a first step toward discovering and studying important interfacial processes with this new nanotechnology tool.

The parallel nanoplotting strategy reported here is not limited to two tips. Indeed, we have shown that a cantilever array consisting of eight tips can be used to generate nanostructures in parallel fashion. In this case, each of the eight tips are coated with ODT. The outermost tip is designated as the imaging tip, and the feedback laser is focused on it during the writing experiment. To demonstrate this concept, we generated four separate nanostructures, a 180-nm dot (contact force  $\sim 0.1$  nN, relative humidity = 26%, contact time = 1 s), a 40-nm-wide line, a square, and an octagon (contact force  $\sim 0.1$  nN, relative humidity  $\sim 26\%$ , writing speed =  $0.5$   $\mu\text{m/s}$ ), and we reproduced these structures in parallel fashion with the seven passively following tips (Fig. 4). Note that there is a less than 10% standard deviation in line width for the original nanostructures and the seven copies.

The number of pens that can be used in a parallel DPN experiment to reproduce nanostructures passively is not limited to eight. Indeed, there is no reason why the number of pens cannot be increased to hundreds or even a thousand pens without the need for additional feedback systems. Finally, this work opens avenues for researchers to begin using DPN and conventional AFM instrumentation to do high-resolution and aligned patterning of nanostructures on a large scale that is automated and moderately fast.

#### References and Notes

1. E. S. Snow, P. M. Campbell, F. K. Perkins, *Appl. Phys. Lett.* **75**, 1476 (1999).
2. R. Luthi *et al.*, *Appl. Phys. Lett.* **75**, 1314 (1999).
3. L. A. Bottomley, *Anal. Chem.* **70**, 425R (1998).
4. J. K. Schoer and R. M. Crooks, *Langmuir* **13**, 2323 (1997).
5. S. Xu and G. Y. Liu, *Langmuir* **13**, 127 (1997).
6. R. M. Nyffenegger and R. M. Penner, *Chem. Rev.* **97**, 1195 (1997).
7. H. Sugimura and N. Nakagiri, *J. Vac. Sci. Technol. A* **14**, 1223 (1996).
8. H. U. Muller, C. David, B. Volkel, M. Grunze, *J. Vac. Sci. Technol. B* **13**, 2846 (1995).
9. Y. Kim and C. M. Lieber, *Science* **257**, 375 (1992).
10. Y. Xia, J. A. Rogers, K. E. Paul, G. M. Whitesides, *Chem. Rev.* **99**, 1823 (1999).
11. R. J. Jackman, J. L. Wilbur, G. M. Whitesides, *Science* **269**, 664 (1995).
12. S. Y. Chou, P. R. Krauss, P. J. Renstrom, *Appl. Phys. Lett.* **67**, 3114 (1995).
13. M. Lutwyche *et al.*, *Sens. Actuators A* **73**, 89 (1999).
14. P. Vettiger *et al.*, *Microelectron. Eng.* **46**, 11 (1999).
15. S. C. Minne *et al.*, *Appl. Phys. Lett.* **73**, 1742 (1998).
16. S. Tsukamoto, B. Siu, N. Nakagiri, *Rev. Sci. Instrum.* **62**, 1767 (1991).
17. R. D. Piner, J. Zhu, F. Xu, S. Hong, C. A. Mirkin, *Science* **283**, 661 (1999).
18. S. Hong, J. Zhu, C. A. Mirkin, *Langmuir* **15**, 7897 (1999).
19. *Science* **286**, 523 (1999).
20. C. A. Mirkin, *MRS Bull.* **2000**, 43 (January 2000).
21. R. D. Piner and C. A. Mirkin, *Langmuir* **13**, 6864 (1997).
22. N. A. Amro, S. X. Xu, G. Y. Liu, *Langmuir* **16**, 3006 (2000).
23. M. Jaschke and H. J. Butt, *Langmuir* **11**, 1061 (1995).

24. Supplementary material is available at [www.sciencemag.org/feature/data/1050099.shl](http://www.sciencemag.org/feature/data/1050099.shl).

25. E. Delamarche *et al.*, *J. Phys. Chem. B* **102**, 3324 (1998).

26. This work was supported by the Air Force Office of Scientific Research, the Defense Advanced Research

Projects Agency, and the NSF-funded Northwestern University Materials Research Center. P. V. Schwartz is acknowledged for helpful discussions.

3 March 2000; accepted 27 April 2000

## Electronic Structure of Mott Insulators Studied by Inelastic X-ray Scattering

M. Z. Hasan,<sup>1\*</sup> E. D. Isaacs,<sup>2</sup> Z.-X. Shen,<sup>1</sup> L. L. Miller,<sup>3</sup> K. Tsutsui,<sup>4</sup> T. Tohyama,<sup>4</sup> S. Maekawa<sup>4</sup>

The electronic structure of Mott insulators continues to be a major unsolved problem in physics despite more than 50 years of research. Well-developed momentum-resolved spectroscopies such as photoemission or neutron scattering cannot probe the full Mott gap. High-resolution resonant inelastic x-ray scattering revealed dispersive charge excitations across the Mott gap in a high-critical temperature parent cuprate ( $\text{Ca}_2\text{CuO}_2\text{Cl}_2$ ), shedding light on the anisotropy of the Mott gap. These charge excitations across the Mott gap can be described within the framework of the Hubbard model.

The discovery of high-critical temperature ( $T_c$ ) superconductivity and colossal magnetoresistance in doped transition metal oxides has led to extensive research interest in Mott insulators. Such oxides are characterized by large onsite Coulomb interaction and the consequent low-temperature insulating state characterized by a charge excitation gap, known as the Mott gap. The gap is either set by the Coulomb interaction  $U$  or the charge transfer energy  $\Delta$  (energy to remove an electron from the oxygen orbital and put it on the copper site), depending on which one is lower ( $I-4$ ). Angle-resolved photoemission spectroscopy (ARPES), which probes only the occupied electronic states, has been remarkably successful in characterizing the electronic structure of cuprate-based insulators ( $5-8$ ). Little is known about the momentum-resolved ( $\mathbf{k}$ -resolved) electronic structure of the unoccupied band, which is a major barrier for a coherent understanding of the nature of the Mott gap and its related insulating state. In addition, knowledge of the unoccupied upper Hubbard band (UHB) is essential to understand the physics of n-type (electron-doped) superconductors, as the doped electrons occupy the UHB. Among the standard probes of condensed matter systems (which allow momentum-resolved studies),

neutrons do not couple to electrons' charge density, and (thermal) neutron energy is too low to reach the Mott edge. No  $\mathbf{k}$ -resolved inverse photoemission (Inv-ARPES) study is available because of problems associated with sample charging as well as the lack of required energy resolution. Inelastic electron scattering, also known as electron energy-loss spectroscopy (EELS), measures electronic excitations from the occupied to the unoccupied bands; however, EELS requires extensive sample preparation and does not yield useful information unless the spectra are corrected for multiple scattering effects ( $9$ ).

Inelastic x-ray scattering is a natural and powerful probe of electronic excitations in condensed matter systems. It has the potential to improve our understanding of the bulk electronic structure of correlated electron systems. Inelastic scattering of x-ray photons covers a fairly wide kinematic range in energy and momentum space, and the photons directly couple to the electronic charge (and to other electronic degrees of freedom, such as orbitals and spins). However, because x-ray photons are highly absorbed in high- $Z$  materials (where  $Z$  is the atomic number), applications of the technique have been mostly limited to low- $Z$  systems ( $10-13$ ). Recent experimental results and theoretical/numerical investigations have shown that by tuning the incident photon energy near an x-ray absorption edge, a Raman-like effect can be measured with nonzero momentum transfer (despite the high absorption cross section) through the large resonant enhancement, which eventually dominates the overall cross section ( $14-19$ ). An inelastically scattered x-ray photon can probe the full charge

<sup>1</sup>Department of Applied Physics, Stanford Synchrotron Radiation Laboratory (SSRL), and Stanford Linear Accelerator Center (SLAC), Stanford University, Stanford, CA 94305, USA. <sup>2</sup>Bell Laboratories, Lucent Technologies, Murray Hill, NJ 07974, USA. <sup>3</sup>Department of Physics and Ames Laboratory, Iowa State University, Ames, IA 50011, USA. <sup>4</sup>Institute of Materials Research, Tohoku University, Sendai 980-8577, Japan.

\*To whom correspondence should be addressed. E-mail: mzhazan@stanford.edu

gap in a Mott insulator through the creation of a hole in the occupied band, thereby promoting an electron across the gap to the unoccupied band with a finite (tunable) momentum transferred into the system. A recent resonant inelastic x-ray scattering (RIXS) study (17) has reported such observation of a low-energy charge transfer gap near 2.5 eV at finite  $\mathbf{q}$  (the scattering wave vector) along the  $\langle 210 \rangle$  direction in a parent cuprate,  $\text{Sr}_2\text{CuO}_2\text{Cl}_2$ , whose electronic structure is similar to that of  $\text{Ca}_2\text{CuO}_2\text{Cl}_2$  (6–8). A similar excitation band has also been reported at finite  $\mathbf{q}$  in EELS (9).

So far, however, no  $\mathbf{q}$ -resolved x-ray study has been reported along the high-symmetry directions. We now report the direct bulk measurement ( $\sim 10$  to  $20 \mu\text{m}$ ) of the electronic excitations in cuprates up to 8 eV energy loss along two high-symmetry directions (the Cu-O bond direction  $\langle 100 \rangle$  and  $45^\circ$  to the bond direction  $\langle 110 \rangle$ ) of the  $\text{CuO}_2$  plane.  $\text{Ca}_2\text{CuO}_2\text{Cl}_2$  was chosen for its relatively low x-ray absorption and high crystalline quality (20). Experiments were performed on the X-21 triple-axis spectrometer at the National Synchrotron Light Source (NSLS), described in detail elsewhere (14, 15). With the incident photon energy fixed on resonance near the Cu K edge at  $E_0$  (incident photon energy) = 8.996 KeV, energy analysis was performed by scanning the analyzer. The overall energy resolution of the spectrometer was 440 meV, as determined by the energy width of the elastic peak. The background, which was measured by keeping track of scattering intensities on the energy gain side, averaged 1 to 2 counts per minute.

Inelastic x-ray scattering spectra in the parent cuprate insulator  $\text{Ca}_2\text{CuO}_2\text{Cl}_2$  with the incident energy near the Cu K $\alpha$  absorption edge ( $E_0 = 8.996 \text{ KeV}$ ) were measured for a range of momentum transfers. The spectra are presented along the  $\langle 110 \rangle$  direction in Fig. 1A and along the  $\langle 100 \rangle$  direction in Fig. 1B. The spectra along the  $\langle 110 \rangle$  direction are taken in the second Brillouin zone, whereas the spectra along the  $\langle 100 \rangle$  direction are in the third Brillouin zone. Selection of different Brillouin zones was due to various kinematic limitations arising from the spectrometer configuration. Each spectrum exhibits two inelastic features: one broad peak around 5.8 eV and a weak feature that disperses with  $\mathbf{q}$  ranging from 2.5 to 3.8 eV. The broad feature centered around 5.8 eV—reported earlier along different directions,  $\langle 001 \rangle$  and  $\langle 210 \rangle$  (15, 17)—changes shape with changing  $\mathbf{q}$  (and polarization) but does not show any significant dispersion in either the  $\langle 100 \rangle$  or  $\langle 110 \rangle$  direction. The lack of dispersion establishes the highly local character of this

excitation. On the basis of electronic structure calculations, the 5.8-eV feature is believed to represent excitations to the unoccupied copper orbitals with antibonding character (15, 21). More precisely, it has been identified as corresponding to a transition from the ground state to a high-energy excited state composed of symmetric contributions of a central  $\text{Cu-}3d_{x^2-y^2}$  orbital and the surrounding  $\text{O-}2p_\sigma$  orbitals (17, 22). In contrast, the position of the lower energy feature changes significantly with  $\mathbf{q}$  from  $(0,0)$  [measured near  $(2\pi, 2\pi)$ ] to  $(\pi, \pi)$ , as seen in Fig. 1A. This feature first emerges clearly from the tail of the elastic peak near  $(\pi/2, \pi/2)$  and disperses upward about 1.35 eV monotonically compared to its position near  $(0,0)$ . At  $\mathbf{q} = (\pi, \pi)$ , where the low-energy excitation has dispersed to 3.8 eV, we note a shoulder of the elastic peak at a lower energy loss near 2.8 eV. With  $\mathbf{q}$  along the  $\langle 100 \rangle$  direction (Fig. 1B), the low-energy feature appears as a shoulder on the elastic peak in the raw data for  $\mathbf{q} < (\pi/2, 0)$ . From  $(\pi/2, 0)$  to  $(\pi, 0)$  it disperses upward by only about 0.56 eV. To make our estimates of the positions of the low-energy inelastic feature more reliable, particularly for low  $\mathbf{q}$ , we removed the elastic peak from the raw data by fitting. Because the subtraction of the fit from the data is imperfect, we do not extract any reliable information about the electronic structure within 1 eV of the elastic peak. Selected spectra with the elastic scattering removed are shown along the  $\langle 110 \rangle$  direction in Fig. 2A and along the  $\langle 100 \rangle$  direction in Fig. 2B. Along the  $\langle 110 \rangle$  direction, dispersion of the low-energy feature is monotonically upward. The spectrum for  $\mathbf{q} = (\pi, \pi)$  (topmost spectrum in

Fig. 2A) shows an even lower energy component near 2.8 eV in addition to the 3.8-eV feature discussed earlier. Along the  $\langle 100 \rangle$  direction, this excitation (the feature's center of gravity) is nearly nondispersive for  $\mathbf{q} < (\pi/2, 0)$  but disperses weakly and monotonically upward for  $\mathbf{q} > (\pi/2, 0)$ . The center of gravity of the low-energy inelastic feature is shown in Fig. 3, A and B, as a function of  $\mathbf{q}$  along the  $\langle 110 \rangle$  and  $\langle 100 \rangle$  directions, respectively. Relative excitation energies are plotted referenced to the energy at  $\mathbf{q} = (0,0)$  along each direction. Because of the doublet nature of the excitation at  $\mathbf{q} = (\pi, \pi)$ , in addition to plotting the center of gravity, we plot the energy position of two separable features. A  $\mathbf{q}$ -space map of charge excitations across the Mott gap is shown in Fig. 3C, which reveals the overall shape of the dispersion surface.

We interpret the low-energy feature in the data as the observation of  $\mathbf{q}$ -resolved excitations across the effective Mott gap, from the occupied band consisting (23) of  $\text{Cu } 3d_{x^2-y^2}$  and  $\text{O-}2p_\sigma$  orbitals [Zhang-Rice band (ZRB)] to the unoccupied UHB along high-symmetry directions. The effective Mott (or charge transfer) excitation is shown in an energy level schematic ( $\mathbf{k}$ -integrated) for this cuprate insulator (Fig. 4A). The RIXS process shakes up the valence electron system and creates a particle-hole pair across the gap, which carries energy and momentum. This pair propagates in a background of antiferromagnetically ordered lattice. In a local picture, the created hole forms a Zhang-Rice singlet (23) and an electron is excited onto the neighboring Cu site occupying the UHB. Figure 4B shows a schematic of a particle-

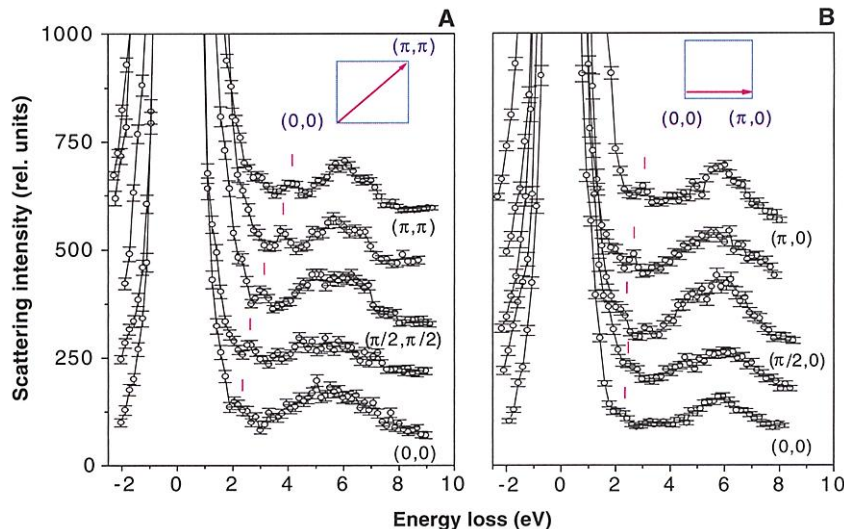


**Fig. 1.** Experimental spectra. The  $\mathbf{q}$  dependences of inelastic x-ray scattering spectra near the Cu K edge are shown along two high-symmetry directions in  $\text{Ca}_2\text{CuO}_2\text{Cl}_2$ : (A) scattering along the  $\langle 110 \rangle$  direction from equivalent  $(0,0)$  to  $(\pi, \pi)$ , and (B) scattering along the  $\langle 100 \rangle$  direction from equivalent  $(0,0)$  to  $(\pi, 0)$ . Incident photon energy  $E_0 = 8.996 \text{ KeV}$ .

hole pair excitation in the  $\text{CuO}_2$  plane (the arrows denote the spins of holes). Strong antiferromagnetic correlation [unusually large superexchange coupling  $J \sim 0.12$  eV (6)] of the system plays a key role in determining the anisotropic propagation of the particle-hole excitations. In addition,

the UHB in cuprates is believed to be strikingly different from the conduction band of a normal semiconductor or a band insulator, as revealed by x-ray absorption spectroscopy (24). We note that in the absence of strong electron-electron correlation, such as in the case of the band insulators, a

convolution of the “valence band” and the “conduction band” is sufficient to understand their RIXS spectra (25). For a Mott insulator, such an approach is not sufficient because the gap does not originate from band effects but rather from the strong correlation effects; hence, the particle-hole excitations of the Mott system cannot be treated as independent excitations of single-particle states (18, 24). Consideration of two-particle Green’s functions is necessary to interpret RIXS spectra. In this sense, RIXS would provide more information than combined ARPES and Invarpes. A model-based rigorous calculation is necessary to elucidate the origin and nature of the  $\mathbf{q}$ -resolved charge excitations in a strongly correlated quantum system.

Several approaches have been proposed to interpret the RIXS process (15–17, 21) in cuprates. The clear dispersions observed along the high-symmetry directions in our experimental data make it possible to perform a direct quantitative comparison to the results of specific many-body model calculations. We consider the Hubbard model with long-range hopping where the lower Hubbard band (LHB) is regarded as the ZRB and the Hamiltonian ( $t$ - $t'$ - $t''$ - $U$  model) is given by

$$H_{3d} = -t \sum_{\langle i,j \rangle, \sigma} (d_{i,\sigma}^\dagger d_{j,\sigma} + \text{h.c.}) - t' \sum_{\langle i,j \rangle', \sigma} (d_{i,\sigma}^\dagger d_{j,\sigma} + \text{h.c.}) - t'' \sum_{\langle i,j \rangle'', \sigma} (d_{i,\sigma}^\dagger d_{j,\sigma} + \text{h.c.}) + U \sum_i n_{i,\uparrow}^d n_{i,\downarrow}^d \quad (1)$$

where  $d_{i,\sigma}^\dagger$  is the creation operator of a 3d electron with spin  $\sigma$  at site  $i$ ,  $n_{i,\sigma}^d = d_{i,\sigma}^\dagger d_{i,\sigma}$ , and  $n_i^d = n_{i,\uparrow}^d + n_{i,\downarrow}^d$ . The summations  $\langle i,j \rangle$ ,  $\langle i,j \rangle'$ , and  $\langle i,j \rangle''$  run over the first, second, and third nearest neighbor pairs, respectively. The values of the parameters are taken from fits to ARPES data on  $\text{Sr}_2\text{CuO}_2\text{Cl}_2$  (8) to be  $t = 0.35$  eV,  $U/t = 10$ ,  $t'/t = -0.34$ , and  $t''/t = 0.23$ , where  $t$ ,  $t'$ , and  $t''$  are the first, second, and third nearest neighbor hopping, respectively, and  $U$  is the on-site Coulomb interaction (8, 18). In the intermediate states of Cu K-edge RIXS process, 3d electrons interact with a 1s core hole created by the dipole transition of a 1s electron to 4p orbital due to the absorption of an incident photon with energy  $\omega_i$  and momentum  $\mathbf{K}_i$ . This interaction Hamiltonian is written as

$$H_{1s-3d} = -V_c \sum_{i,\sigma,\sigma'} n_{i,\sigma}^d n_{i,\sigma'}^s \quad (2)$$

where  $n_{i,\sigma}^s$  is the number operator of 1s core hole with spin  $\sigma$  at site  $i$ , and  $V_c$  (coupling between the core-hole and the 3d electron system) is taken to be positive. This interaction causes excitations of the 3d electrons across the gap. The photoexcited 4p electron is assumed to go into the bottom of the 4p band and not to interact with either the 3d electrons or the 1s core hole because of the

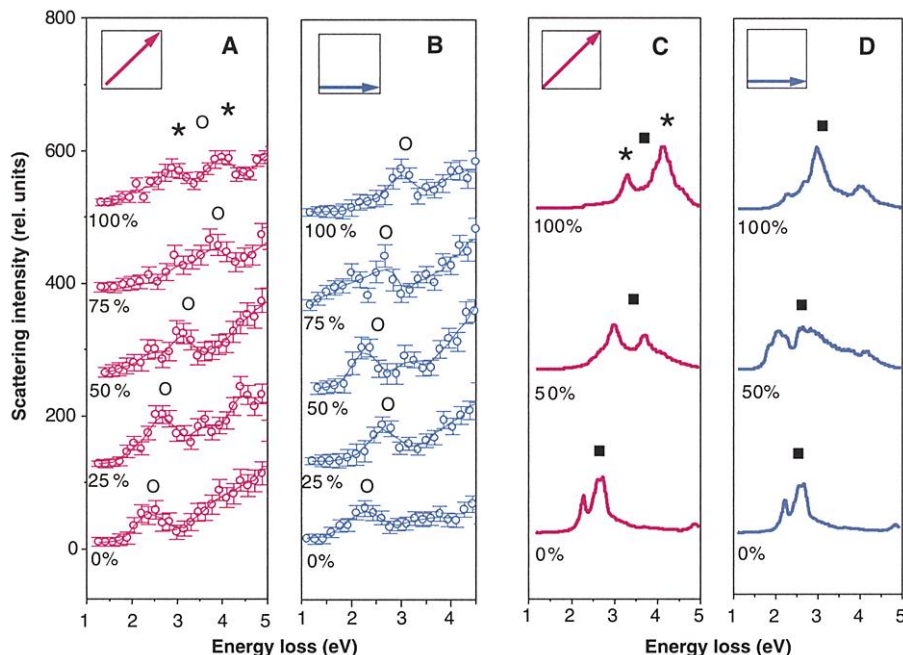


**Fig. 2.** Extracted data and model comparison. Momentum dependences of the RIXS spectra are compared with Hubbard model calculations: The experimental spectra (with elastic scattering removed) are shown along the  $\langle 110 \rangle$  direction (A) and the  $\langle 100 \rangle$  direction (B), and the calculated ones (low-energy component only) are along the  $\langle 110 \rangle$  direction (C) and the  $\langle 100 \rangle$  direction (D). The parameter values for (C) and (D) are  $t = 0.35$  eV,  $U/t = 10$ ,  $t'/t = -0.34$ ,  $t''/t = 0.23$ , and  $V_c/t = 15$  (8, 18). The centers of gravity of spectral weights are indicated by open circles for the experimental data and closed squares for the  $t$ - $t'$ - $t''$ - $U$  Hubbard model calculations; the pairs of asterisks in (A) and (C) indicate the center of gravity of two features on the topmost spectra. The percentages show the normalized  $\mathbf{q}$  coordinates (locations inside the Brillouin zone), and the inset in each panel shows the direction of the scattering wave vector  $\mathbf{q}$  (the momentum transfer).

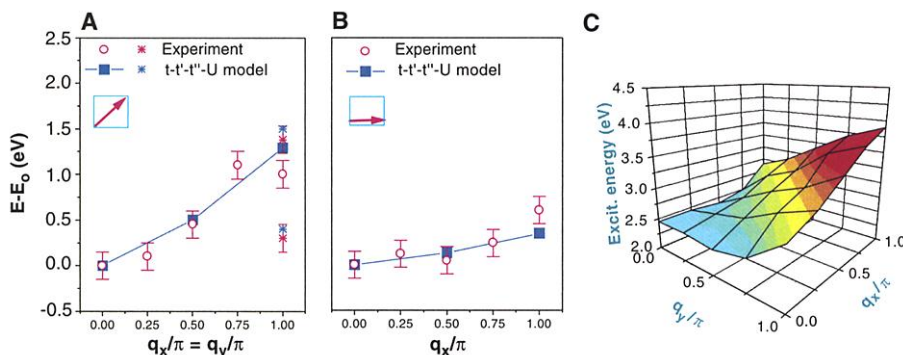


**Fig. 3.** Dispersion plots. The experimental and theoretical results on the momentum dependence of the center of gravity of the low-energy inelastic feature are shown along the  $\langle 110 \rangle$  direction (A) and the  $\langle 100 \rangle$  direction (B). Relative excitation energies are plotted referenced to the energy at  $\mathbf{q} = (0,0)$  along each direction. Open magenta circles and closed cyan squares denote experimental and theoretical centers of gravity, respectively. For  $\mathbf{q} = (\pi, \pi)$  [in (A), fractional  $\mathbf{q}$  coordinate = 1], in addition to plotting the center of gravity, we plot the locations of two separable features denoted by asterisks for data (magenta) and theory (cyan). (C) A  $\mathbf{q}$ -space map of charge excitations across the Mott gap, which summarizes the overall dispersion behavior. [The color in (C) recodes the energy axis to create a clear visual representation for the shape of the dispersion surface.]

delocalized nature of the 4p bands. In the final state, the 4p electron goes back to the 1s orbital, emitting a photon with energy  $\omega_f$  and momentum  $\mathbf{K}_f$ . It is also assumed that the momentum transfer,  $\mathbf{q} = \mathbf{K}_i - \mathbf{K}_f$ , is conserved within the electronic degrees of freedom. In this scenario, the RIXS spectrum is given by

$$I(\mathbf{q}, \Delta\omega) = \sum_{\alpha} |\langle \alpha | \sum_{\sigma} s_{\mathbf{k}0-\mathbf{K}_f, \sigma} p_{\mathbf{k}0, \sigma} (H + \varepsilon_{1s-4p} - E_0 - \omega_i - i\Gamma)^{-1} p_{\mathbf{k}0, \sigma}^{\dagger} s_{\mathbf{k}0-\mathbf{K}_i, \sigma}^{\dagger} | 0 \rangle |^2 \delta(\Delta\omega - E_{\alpha} + E_0) \quad (3)$$

(18), where  $H = H_{3d} + H_{1s-3d}$ ,  $\mathbf{q} = \mathbf{K}_i - \mathbf{K}_f$ ,  $\Delta\omega = \omega_i - \omega_f$ ,  $s_{\mathbf{k}, \sigma}^{\dagger}$  ( $p_{\mathbf{k}, \sigma}^{\dagger}$ ) is the creation operator of the 1s core hole (4p electron) with momentum  $\mathbf{k}$  and spin  $\sigma$ ,  $|0\rangle$  is the ground state of the half-filled system with energy  $E_0$ ,  $|\alpha\rangle$  is the final state of the RIXS process with energy  $E_{\alpha}$ ,  $\Gamma$  is the inverse of the relaxation time in the intermediate state, and  $\varepsilon_{1s-4p}$  is the energy difference between the 1s level and the bottom of the 4p band. The values of the parameters are set to be  $V_0/t = 15$  and  $\Gamma/t = 1$  (18).

The RIXS spectra calculated on a  $4 \times 4$  site cluster are shown in Fig. 2, C and D. Along the  $\langle 110 \rangle$  direction, the energy position of the features increases monotonically with increasing  $\mathbf{q}$ . In contrast to the  $\langle 110 \rangle$  direction, the spectral threshold along the  $\langle 100 \rangle$  direction decreases in energy from  $\mathbf{q} = (0,0)$  to  $(\pi/2,0)$ , and then increases toward  $\mathbf{q} = (\pi,0)$ . These features are consistent with the low-energy features of the experimental spectra (Fig. 2, A and B). For more quantitative comparison between experiment and model, we plotted the momentum dependence of the center of gravity of the experimental and numerical results (Fig. 3, A and B). Along the  $\langle 110 \rangle$  direction, the overall trend of the center of

gravity is similar between the experiment and the model. For the  $\mathbf{q} = (\pi, \pi)$  spectrum, we plot two centers of gravity due to two separable low-energy features (Fig. 2A, top spectrum). Note that the theory curve at  $\mathbf{q} = (\pi, \pi)$  also contains two features that are most separated in energy (Fig. 2C, top spectrum). The lower energy peak near 2.8 eV in the “doublet” seen for  $\mathbf{q} = (\pi, \pi)$  (Fig. 2A, top spectrum) is likely to be of excitonic origin, indicating the possibility of intersite Coulomb correlations. Along the  $\langle 100 \rangle$  direction, the correspondence of the centers of gravity between experiment and theory is also reasonably good. The flatness in energy dispersion from  $\mathbf{q} = (0,0)$  to  $(\pi/2,0)$  (Fig. 3B) is probably because in the  $t-t'-t''-U$  model—that is, in the presence of higher order hopping—the single-particle spectral function  $[A(\mathbf{k}, \omega)]$  for the unoccupied states (UHB) has a minimum near  $\mathbf{k} = (\pi, 0)$ , unlike the occupied ZRB’s maximum, which is near  $\mathbf{k} = (\pi/2, \pi/2)$  (6, 7, 9, 22). Such flatness is not expected in the  $t-U$  model (18, 26). Hence, our results suggest that the unoccupied band has a different symmetry relative to the occupied band. This disparity between the occupied and the unoccupied bands may shed light on the origin of the different behaviors of n-type and p-type cuprate superconductors. At this level of experimental resolution, it is not necessary to consider different values for the hoppings between the ZRB and the UHB to describe these results. Further high-resolution work is necessary to resolve the details of many of these issues. We conclude that these results, in general, indicate that the  $\mathbf{q}$ -resolved charge excitations across the Mott gap can be described within the general framework of the standard Hubbard model.

Our results demonstrate the power and versatility of x-ray spectroscopy, and its superiority to other well-developed spectroscopic techniques, in addressing some fundamental issues of charge excitation in Mott insulators. The availability of brighter synchrotron sources with higher resolution would permit a more detailed study of various aspects of Mott insulators, such as the possibility of the broken particle-hole symmetry (as hinted here), the magnitude of intersite Coulomb coupling, and charge correlations in an RVB-like (27) state. The feasibility of such experiments points to the opening of a new frontier of correlated systems research.

## References and Notes

- N. F. Mott, *Proc. Phys. Soc. London Ser. A* **62**, 416 (1949).
- J. Hubbard, *Proc. Phys. Soc. London Ser. A* **277**, 237 (1964).
- P. W. Anderson, *Phys. Rev.* **115**, 2 (1959).
- J. Zaanen, G. A. Sawatzky, J. W. Allen, *Phys. Rev. Lett.* **55**, 418 (1985).
- Z. X. Shen *et al.*, *Science* **267**, 343 (1995).
- F. Ronning *et al.*, *Science* **282**, 2067 (1998).
- S. LaRosa *et al.*, *Phys. Rev. B* **56**, R525 (1997).
- C. Kim *et al.*, *Phys. Rev. Lett.* **80**, 4245 (1998).
- Y. Y. Wang *et al.*, *Phys. Rev. Lett.* **77**, 1809 (1996).
- J. P. Hill *et al.*, *Phys. Rev. Lett.* **77**, 3665 (1996).
- E. D. Isaacs, P. M. Platzman, P. Metcalf, J. M. Honig, *Phys. Rev. Lett.* **76**, 4211 (1996).
- F. Sette *et al.*, *Phys. Rev. Lett.* **77**, 83 (1996).
- E. D. Isaacs and P. M. Platzman, *Phys. Today* **49**, 40 (1996).
- C. C. Kao, W. A. L. Caliebe, J. B. Hastings, J. M. Gillet, *Phys. Rev. B* **54**, 16361 (1996).
- J. P. Hill *et al.*, *Phys. Rev. Lett.* **80**, 4967 (1998).
- P. M. Platzman and E. D. Isaacs, *Phys. Rev. B* **57**, 11107 (1998).
- P. Abbamonte *et al.*, *Phys. Rev. Lett.* **83**, 860 (1999).
- K. Tsutsui, T. Tohyama, S. Maekawa, *Phys. Rev. Lett.* **83**, 3705 (1999).
- K. Tsutsui *et al.*, <http://xxx.lanl.gov/abs/cond-mat/9909346>.
- L. L. Miller *et al.*, *Phys. Rev. B* **41**, 1921 (1990).
- T. Ide and A. Kotani, *J. Phys. Soc. Jpn.* **68**, 3100 (1999).
- M. E. Simon *et al.*, *Phys. Rev. B* **54**, R3780 (1996).
- F. C. Zhang and T. M. Rice, *Phys. Rev. B* **37**, 3759 (1988).
- H. Romberg, M. Alexander, N. Nucker, P. Adelmann, J. Fink, *Phys. Rev. B* **42**, 8768 (1990).
- E. L. Shirley, in *Raman Emission by X-Ray Scattering*, D. L. Ederer and J. H. McGuire, Eds. (World Scientific, New Orleans, 1996), pp. 51–52.
- K. Tsutsui, T. Tohyama, S. Maekawa, unpublished data.
- P. W. Anderson, *Science* **235**, 1996 (1987).
- P. Horsch *et al.*, *Physica C* **162–164**, 783 (1989).
- We thank P. Abbamonte, G. Aeppli, S. Ahmed, P. W. Anderson, N. P. Armitage, A. I. Bienenstock, P. Bogdanov, C. A. Burns, S. Doniach, D. L. Feng, Z. Hussain, C. C. Kao, S. A. Kivelson, M. V. Klein, R. B. Laughlin, P. B. Littlewood, V. Oganesyan, P. M. Platzman, F. Ronning, G. A. Sawatzky, K. M. Shen, J. Zaanen, S. C. Zhang, and X. Zhou for useful suggestions. The work at NSLS/Brookhaven was jointly supported by Bell Labs, Lucent Technologies, and the U.S. Department of Energy/Basic Energy Sciences (Materials Sciences Division). The theoretical/numerical work was supported by Priority-Areas Grants from the Ministry of Education, Science, Culture and Sport of Japan, Core Research for Evolutional Science and Technology, and New Energy and Industrial Technology Development Organization. Computations were carried out at the Institute of Solid State Physics (University of Tokyo) and Institute of Materials Research (Tohoku University).

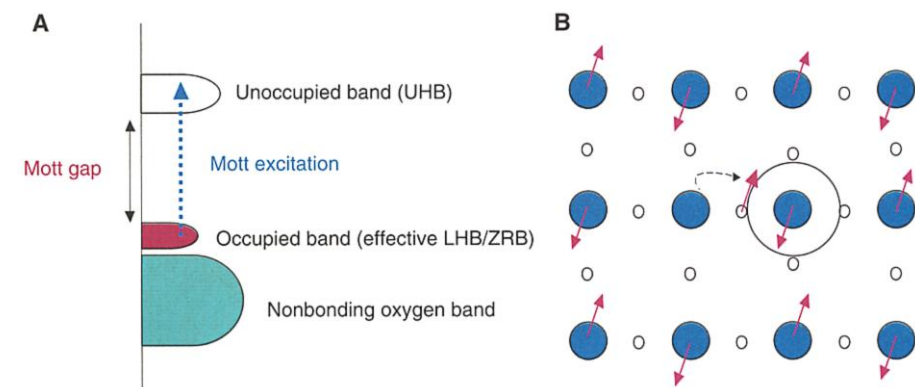


**Fig. 4.** Mott excitation cartoons. **(A)** Schematic of ( $\mathbf{k}$ -integrated) electronic structure of the parent copper oxide insulator. There exists a charge excitation gap between the occupied band and the unoccupied UHB (23, 28). The arrow denotes the excitation of an electron. **(B)** Schematic of particle-hole pair excitations in a  $\text{CuO}_2$  square lattice with long-range antiferromagnetic correlation. The arrows denote the spins of holes. The filled dark cyan and empty white circles denote Cu sites and O sites, respectively. The (dark cyan) empty site in the middle is the electron (particle), and the large complex containing four oxygen sites is the Zhang-Rice singlet (hole) (9). The experimental results reveal that the propagation of particle-hole excitations is strongly anisotropic in this antiferromagnetically ordered lattice.

9 February 2000; accepted 20 April 2000